The enterocyte microvillus is a vesicle-generating organelle

Russell E. McConnell,[1] James N. Higginbotham,[2] David A. Shifrin Jr.,[1] David L. Tabb,[4] Robert J. Coffey,[1,2,3] and Matthew J. Tyska[1]

[1]Department of Cell and Developmental Biology, [2]Department of Medicine, [3]Department of Veterans Affairs Medical Center, and [4]Department of Biomedical Informatics, Vanderbilt University Medical Center, Nashville, TN, 37232

For decades, enterocyte brush border microvilli have been viewed as passive cytoskeletal scaffolds that serve to increase apical membrane surface area. However, recent studies revealed that in the in vitro context of isolated brush borders, myosin-1a (myo1a) powers the sliding of microvillar membrane along core actin bundles. This activity also leads to the shedding of small vesicles from microvillar tips, suggesting that microvilli may function as vesicle-generating organelles in vivo. In this study, we present data in support of this hypothesis, showing that enterocyte microvilli release unilamellar vesicles into the intestinal lumen; these vesicles retain the right side out orientation of microvillar membrane, contain catalytically active brush border enzymes, and are specifically enriched in intestinal alkaline phosphatase. Moreover, myo1a knockout mice demonstrate striking perturbations in vesicle production, clearly implicating this motor in the in vivo regulation of this novel activity. In combination, these data show that microvilli function as vesicle-generating organelles, which enable enterocytes to deploy catalytic activities into the intestinal lumen.

Introduction

The small intestinal epithelial cell (enterocyte) brush border is a highly ordered cellular specialization that functions as a primary site of nutrient processing and absorption as well as the major barrier to the resident intestinal microbiota and to pathogens introduced into the gastrointestinal tract (Mooseker, 1985). The brush border of a single cell consists of thousands of tightly packed microvilli that extend off of the apical cell surface. Each microvillus consists of a cylindrical membrane protrusion (~100-nm diameter × 1–2-µm long) that is supported by a polarized bundle of actin filaments oriented with plus ends extending into the tip (Mooseker and Tilney, 1975). These core bundles are held together with the cross-linking proteins villin, fimbrin, and espin (Revenu et al., 2004), which provide mechanical stability and regulate the dynamics of actin turnover (Loomis et al., 2003). The obvious structural consequence of this distinctive arrangement is that a brush border can accommodate ~100-fold more membrane than a flat surface would afford; the coordinate functional consequence is an immense capacity for housing various membrane-bound transporters and channels that endow the brush border with its absorptive properties. Indeed, the functional significance of normal brush border structure is underscored by the fact that disruption of brush border membrane organization is associated with several pathological conditions, including microvillus inclusion disease (Cutz et al., 1989) and gluten-sensitive enteropathies such as Celiac Disease (Iancu and Elian, 1976; Bailey et al., 1989).

Within enterocyte microvilli, the plasma membrane is connected to the core actin bundle by the motor protein myosin-1a (myo1a) (Mooseker and Tilney, 1975; Mooseker and Coleman, 1989). As alluded to in the previous paragraph, enterocyte microvilli have historically been viewed as passive cytoskeletal scaffolds that increase apical membrane surface area, thereby enhancing the nutrient processing and absorptive capacity of the intestinal epithelium (Brown, 1962). However, recent findings have challenged this model by demonstrating that in isolated brush borders, myo1a is able to propel microvillar membrane over core actin bundles (McConnell and Tyska, 2007). This movement results in the shedding of membrane from

Correspondence to Matthew J. Tyska: matthew.tyska@vanderbilt.edu

Abbreviations used in this paper: DPPIV, dipeptidyl peptidase IV; FAVS, fluorescence-activated vesicle sorting; IAP, intestinal alkaline phosphatase; KO, knockout; LPH, lactase-phlorizin hydrolase; LPS, lipopolysaccharide; LV, lumenal vesicle; MGAM, maltase glucoamylase; MS, mass spectrometry; myo1a, myosin-1a; PI-PLC, phosphatidylinositol-specific PLC; SEM, scanning EM; SI, sucrase isomaltase; TEM, transmission EM; WT, wild type.

The Rockefeller University Press $30.00
J. Cell Biol. Vol. 185 No. 7 1285–1298
www.jcb.org/cgi/doi/10.1083/jcb.200902147

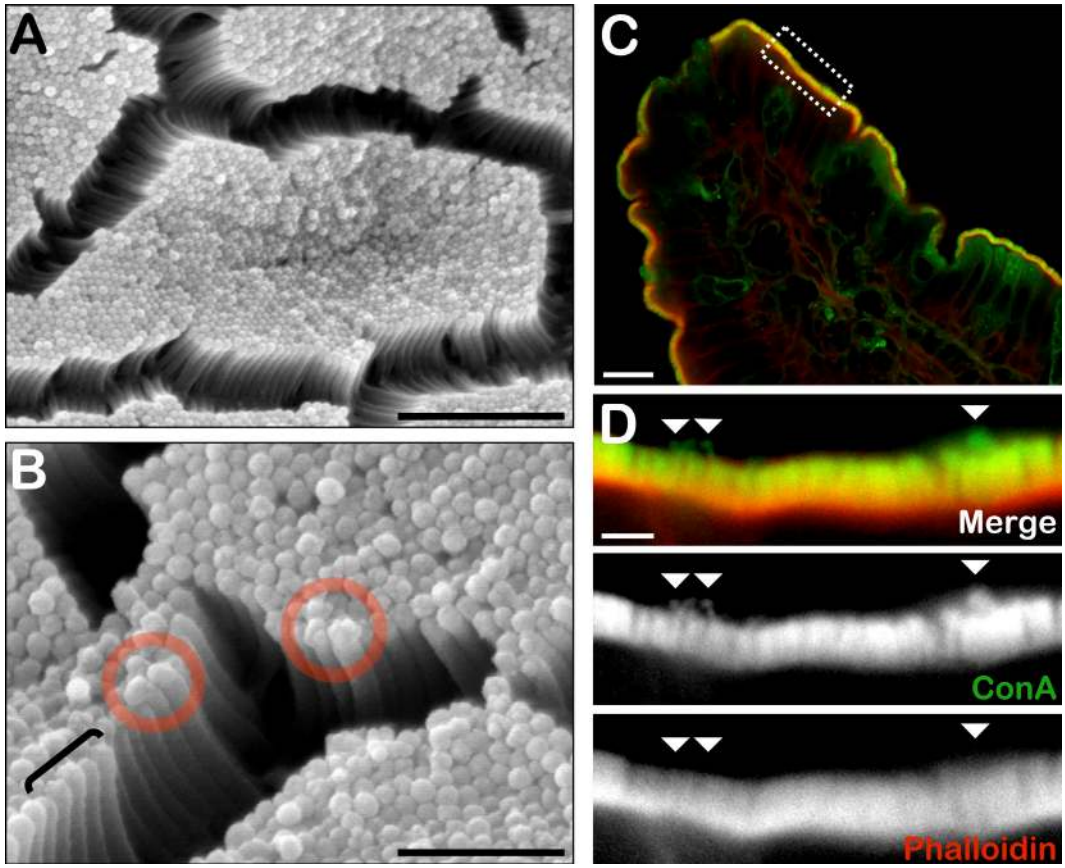

Figure 1. **Bulbous membrane protrusions are observed at microvillar tips.** (A) SEM micrograph of the duodenum lumenal surface shows the presence of membrane extensions at the tips of large numbers of enterocyte microvilli. Membrane bulbs displayed a mean diameter of 102.5 ± 13.1 nm (n = 100). Bar, 1.6 µm. (B) A higher magnification view of the enterocyte apical surface reveals that some microvilli demonstrate characteristically regular height and tip diameter (bracket), whereas others have enlarged or irregular tips (red circles). Bar, 0.6 µm. (C) Low magnification confocal micrograph of a section through a small intestine villus labeled with fluorescent conjugates of the lectin Alexa Fluor 488–Con A (green) and the filamentous actin–binding protein Alexa Fluor 633–phalloidin (red) to mark membranes and actin, respectively. Enterocyte brush borders line the lumenal surface of the villus and are visualized as the strongly labeled yellow band at the villus perimeter. Bar, 10 µm. (D) A high magnification view of the boxed area in C is shown. Small membrane bulbs protruding from the tips of microvilli can be seen (arrowheads). Note that the membrane bulbs do not contain actin filaments. Bar, 2 µm.

microvillar tips in the form of small (~100-nm diameter) unilamellar vesicles, raising the intriguing possibility that microvilli might function as active, vesicle-generating organelles. Because the brush border is positioned at the enterocyte–lumen interface, the shedding of microvillar membrane could represent an important aspect of enterocyte functions that involve communicating with and/or conditioning the lumenal environment (Jacobs, 1983; Bates et al., 2007; Goldberg et al., 2008).

As our initial experiments were limited to in vitro observations using isolated brush borders (McConnell and Tyska, 2007), the possibility that microvilli function as vesicle-generating organelles has not been explored. Thus, the goal of this study was to combine light microscopy and EM with biochemical and proteomic approaches to investigate this hypothesis. Our findings clearly show that native microvilli are capable of releasing vesicles from their distal tips in vivo. The resulting vesicles contain several catalytically active enzymes normally associated with the brush border but are specifically enriched in intestinal alkaline phosphatase (IAP). In a manner consistent with our previously published in vitro data (McConnell and Tyska, 2007), we find that myo1a knockout (KO) mice demonstrate marked defects in vesicle production. Based on these data, we propose that enterocyte microvilli function as active vesicle-generating organelles. This novel aspect of epithelial cell biology may enable enterocytes to distribute specific enzyme activities into the intestinal lumen to serve in nutrient processing and/or host defense.

Results

Bulbous protrusions of apical membrane are found at microvillar tips in vivo

Although our previous experiments indicate that microvilli hold the potential to produce vesicles (McConnell and Tyska, 2007), these experiments were performed with isolated brush borders. If microvilli do produce vesicles in vivo, one would expect to observe morphological evidence of this process at the level of individual microvilli in the context of native intestinal tissue samples. To test this prediction, we examined rat small intestine using scanning EM (SEM), an approach well suited for the visualization of cell surface features. High magnification (50,000×) observations in ad libitum–fed adult rat duodenum revealed the presence of bulbous membrane protrusions at the distal tips of microvilli with a mean diameter of 102.5 ± 13.1 nm (Fig. 1, A and B). Although not present

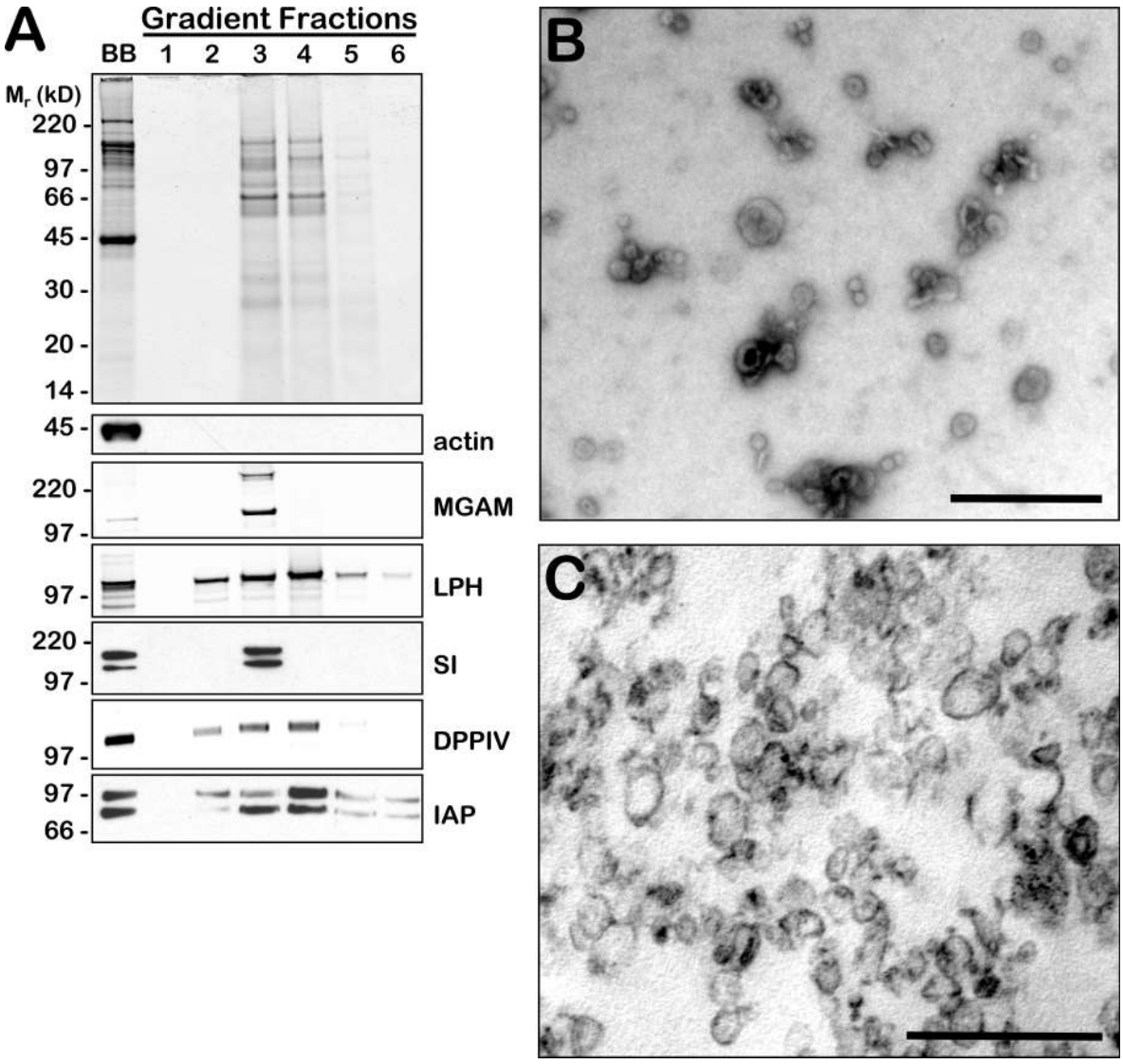

Figure 2. **Isolation of vesicles from the intestinal lumen.** (A) Lumenal contents from rat small intestine were fractionated using differential centrifugation (see Materials and methods); the resulting 100,000 *g* pellet was resuspended and loaded onto a discontinuous sucrose gradient. A Coomassie blue–stained gel of the gradient fractions shows that most of the protein is found in fractions 3 and 4. Western blot analysis reveals that fraction 3 contains several membrane proteins that are found at high levels in the enterocyte microvillar membrane (MGAM, LPH, SI, DPPIV, and IAP) and does not have detectable levels of actin. (B) Negative-stain TEM of fraction 3 shows the presence of membrane structures in the intestine lumenal contents that are similar in size to the membrane accumulations observed at the tips of microvilli. (C) Ultrathin sections of fraction 3 viewed by TEM clearly show that the majority of vesicles present in this fraction are unilamellar. Bars, 0.5 µm.

on the tip of every microvillus, these protrusions or "bulbs" appeared to be ubiquitous, as they were present on the surface of enterocytes along the length of a given villus. Apical membrane bulbs were also observed in confocal micrographs of intestinal frozen sections fluorescently labeled with Con A and phalloidin to mark the apical membrane and actin filaments, respectively (Fig. 1, C and D). These images clearly show membrane protruding from enterocytes into what would be lumenal space (Fig. 1 D, arrowheads). Importantly, bulbs were devoid of phalloidin signal, ruling out the possibility that these structures simply represent microvilli of above average length.

The membrane bulbs imaged in both SEM and confocal micrographs (Fig. 1, B [red circles] and D [arrowheads]) bear a striking resemblance to the vesiculating membrane observed at microvillar tips of isolated brush borders after ATP exposure (McConnell and Tyska, 2007). Thus, distal tip bulbs may represent structural intermediates in the process of microvillar membrane shedding.

Vesicles containing microvillar membrane markers are found in the intestinal lumen

Vesicles released from the tips of microvilli in vivo should accumulate in the intestinal lumen. To determine whether such vesicles are present, full lengths of small intestine were dissected out of adult rats and flushed with saline; the resulting lumen wash was then fractionated using differential and gradient centrifugation. Gradient fractions were assayed for the presence of enterocyte-derived vesicles using negative-stain transmission EM (TEM) and Western blot analysis using antibodies directed against

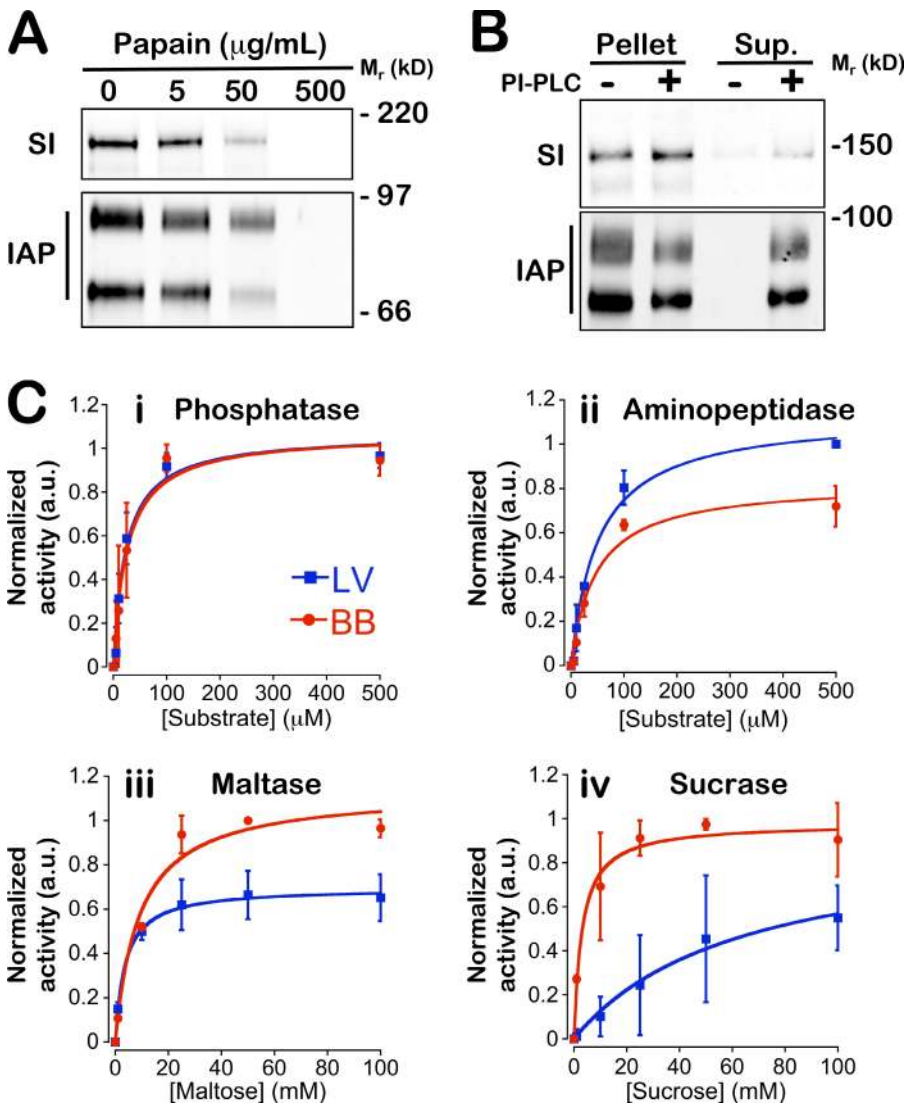

Figure 3. **LVs are oriented right side out and exhibit catalytic activity.** (A) Intact LVs were incubated with increasing concentrations of papain-conjugated beads, the beads were removed with centrifugation (500 *g*), and the supernatant was centrifuged (100,000 *g*) to pellet LVs. Western blot analysis of the 100,000 *g* pellet shows that both IAP and SI are cleaved from LVs by papain, with neither protein being detectable in the 100,000 *g* pellet at the highest papain concentration. (B) LVs incubated with PI-PLC for 15 min at 30°C were pelleted with ultracentrifugation (100,000 *g*), and membrane protein distributions were examined by Western blotting. In control samples (−), IAP and SI were found entirely in the pellet fraction. PI-PLC treatment (+) released approximately half of the IAP from the pellet into the supernatant. The transmembrane protein SI was unaffected by PI-PLC treatment, remaining in the pellet in both control (−) and PI-PLC–treated (+) samples. (C) The enzyme activities of intact LVs (25 μg; blue squares) were compared with isolated brush borders (25 μg; red circles) using the fluorescent substrates 4-methylumbelliferyl phosphate (i) and *H*-Leu-7-amino-4-methylcoumarin (ii) to measure phosphatase and aminopeptidase activities, respectively. To assess disaccharidase activities, samples were incubated with maltose (iii) and sucrose (iv), and liberated glucose was measured using a hexokinase assay (Sigma-Aldrich). LVs demonstrated robust phosphatase and aminopeptidase activities (i and ii) but possessed significantly less maltase (iii) and sucrase (iv) activities ($P < 0.05$). Data are presented as mean ± standard error of the mean. Error bars show fits to a Michaelis–Menten model: normalized activity = (V_{Max} × [substrate])/(K_M + [substrate]).

microvillar membrane components (Fig. 2). Gradient fraction 3, which included the 16–25% sucrose interface, was highly enriched in unilamellar vesicles with a size comparable with the diameter of microvilli (~100 nm), as observed using negative stain and ultrathin section TEM (Fig. 2, B and C). Western blotting revealed that this lumenal vesicle (LV) fraction contains several integral membrane proteins that are expressed in enterocytes and found in the brush border, including maltase glucoamylase (MGAM), lactase-phlorizin hydrolase (LPH), sucrase isomaltase (SI), dipeptidyl peptidase IV (DPPIV), and IAP (Fig. 2 A). Importantly, actin was not detectable in any of the gradient fractions, indicating that vesicles at the 16–25% interface are not likely the result of microvillar/brush border fragmentation. These data show that small vesicles, which may be derived from the microvillar membrane, are in fact found in the intestinal lumen.

LV membranes are oriented right side out

Based on our in vitro experiments, vesicles released during microvillar membrane shedding are expected to retain the orientation of the native microvillar membrane (McConnell and Tyska, 2007). To determine whether LVs are oriented "right side out," vesicles were mixed with papain-conjugated beads to cleave exposed proteins from the vesicle surface (Maestracci, 1976). After papain treatment, LVs were centrifuged (100,000 *g*) and the pellet analyzed by Western blotting. Increasing concentrations of papain resulted in progressively more protein cleavage; at the highest papain concentration, IAP and SI were completely lost from the LV pellet (Fig. 3 A). Similarly, phosphatidylinositol-specific PLC (PI-PLC) released the glycosylphosphatidylinositol-anchored protein IAP from the LV pellet into the supernatant without affecting the transmembrane protein SI (Fig. 3 B). These data show that LV membrane proteins are surface exposed and suggest that LVs are right side out; i.e., LV membrane has the same orientation as microvillar membrane.

LV-associated enzymes are catalytically active

Given the right side out orientation of vesicles in the LV fraction, component enzymes should have access to substrates present in the lumen and may therefore exhibit catalytic activities. We investigated the presence of enzyme activities in the LV fraction

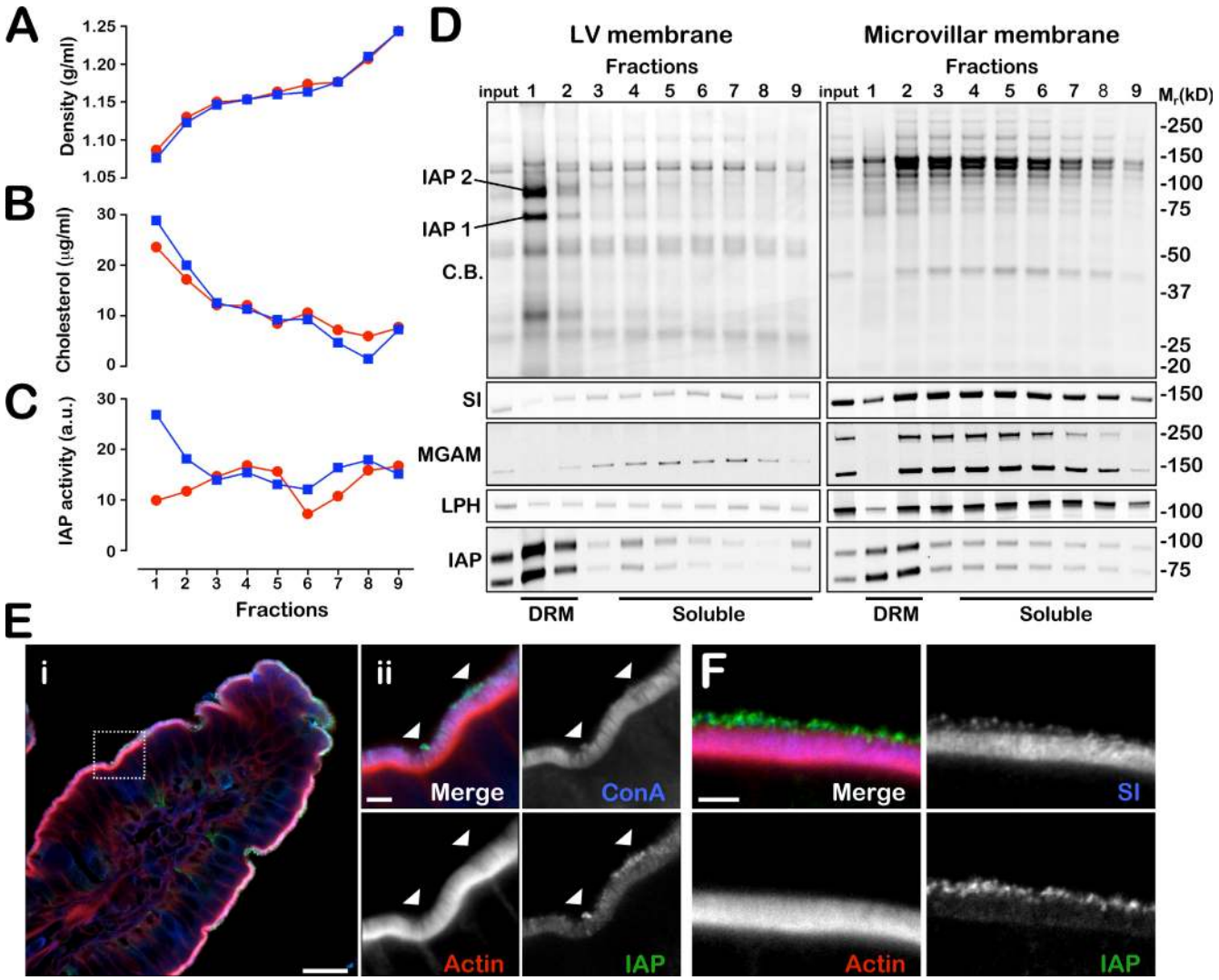

Figure 4. **LVs are specifically enriched in IAP.** (A) LVs and microvillar membrane were extracted with 1% NP-40 on ice and loaded onto self-forming Optiprep density gradients. Density profiles of 30% Optiprep density gradients are shown. (B) Optiprep gradient fractions of LV and microvillar membrane were analyzed using an Amplex Red Cholesterol Assay kit (Invitrogen). Cholesterol from both samples distributed similarly, showing obvious enrichment in the low density fractions (fractions 1 and 2). (C) IAP enzyme activity was assayed using the quenched fluorescent substrate phenylumbelliferyl phosphate. LV Optiprep gradient fraction 1 demonstrated the highest phosphatase activity, with considerably less activity detected in the microvillar membrane fractions. (A–C) Blue squares, LVs; red circles, microvillar membrane. (D) Optiprep gradient fractions were separated using SDS-PAGE. Coomassie blue (CB)–stained gels show the distribution of LV and microvillar membrane proteins between detergent-resistant membrane (DRM) and detergent-soluble fractions (loaded for equal volume). The two prominent bands observed in LV fraction 1 were excised and identified by MS as the two isoforms of IAP found in rat. Western blot analysis confirmed the enrichment of IAP in this fraction, while demonstrating that the enterocyte membrane proteins SI, MGAM, and LPH were depleted in LVs relative to microvillar membrane. (E) Confocal micrographs of sections through small intestine villi labeled with Alexa Fluor 488–Con A (blue), Alexa Fluor 633–phalloidin (red), and an antibody directed against IAP (Alexa Fluor 568; green). (ii) A high magnification view of the boxed area in i shows that Con A–labeled membrane extensions are enriched in IAP and devoid of actin staining (arrowheads). IAP enrichment was observed in membrane extensions found at the tips of microvilli in every villus examined (n = 30). Bars: (i) 20 μm; (ii) 2 μm. (F) Confocal micrographs of sections through small intestine villi labeled with Alexa Fluor 633–phalloidin (red) and antibodies directed against IAP (green) and SI (blue). The obvious enrichment of IAP at the microvillus tip is in stark contrast to SI, which localizes predominantly along the actin-supported length of the microvillus. Bar, 2 μm.

using substrates specific to common brush border hydrolases. Strikingly, LVs possessed activities comparable with brush border controls with nearly identical IAP and aminopeptidase activities in assays loaded for equal total protein (Fig. 3 C, i and ii). Although LVs did possess disaccharidase activities, these were significantly lower than those of isolated brush borders (Fig. 3 C, iii and iv). These results demonstrate that LV-associated enzymes are catalytically active and suggest that LV production may be a means of distributing specific enzymatic activities into the intestinal lumen.

LVs are specifically enriched in IAP

To further develop insight into LV function, we sought to determine which LV-associated proteins were enriched or depleted relative to the composition of whole microvillar membrane. When detergent-extracted LV and microvillar membranes were separated using 30% iodixanol gradients (Optiprep; Sigma-Aldrich), the resulting fractions demonstrated comparable cholesterol distributions (Fig. 4, A and B). Western blot analysis of gradient fractions revealed that LV and microvillar membrane proteins undergo similar partitioning between detergent-resistant

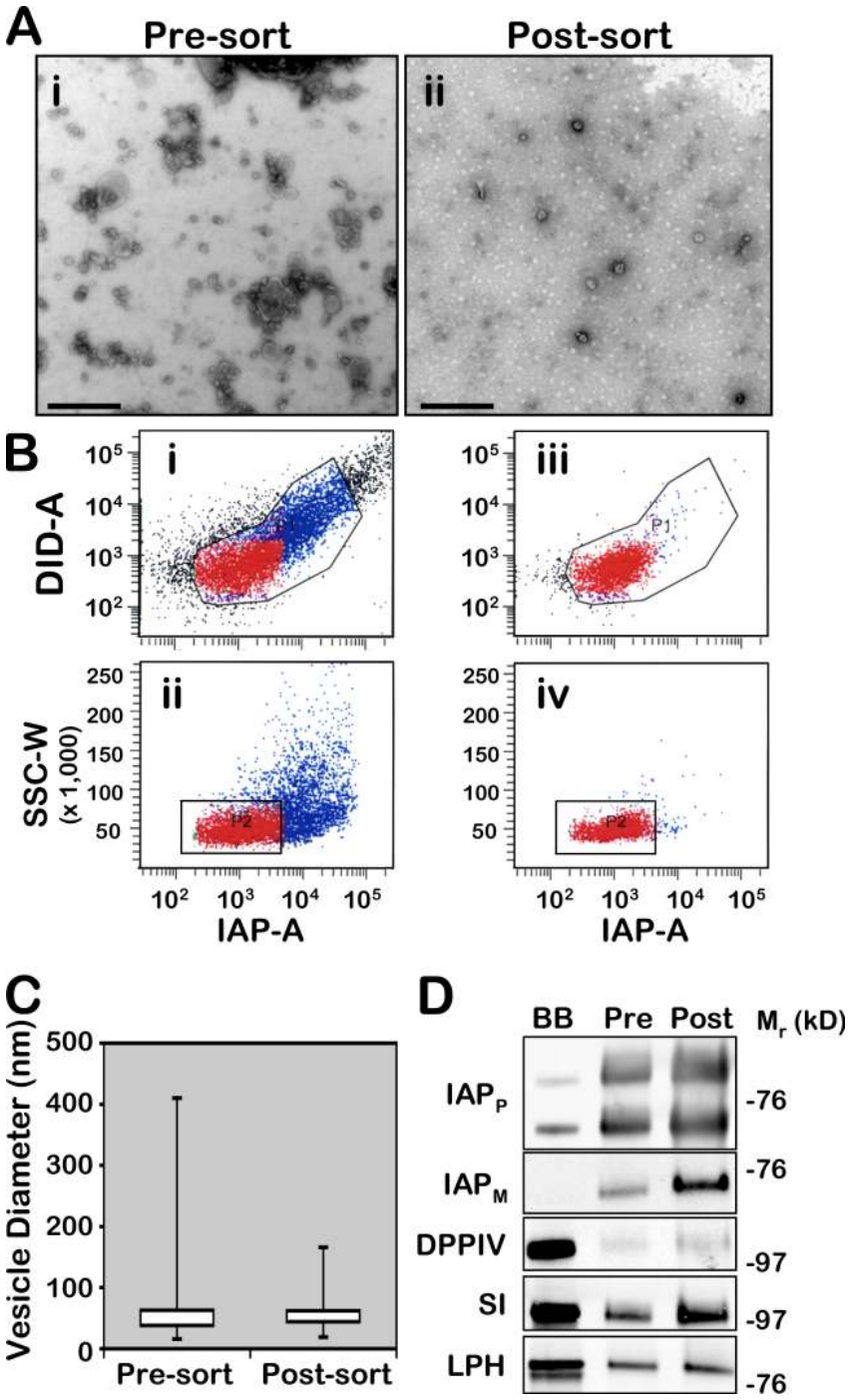

Figure 5. **Purification of IAP-enriched LVs by FAVS.** (A) Negative-stain TEM of vesicles present in sucrose gradient fraction 3. The considerable size variation observed before FAVS (i) is notably decreased after sorting (ii). Bars, 0.5 µm. (B) Fraction 3 vesicles were labeled with the lipophilic dye DiD and an Alexa Fluor 488 antibody to detect IAP as outlined in Materials and methods. Light-scattering properties were used to eliminate large particles or aggregates. Particles within established gates (black outlines; red denotes particles included in all gates) were isolated for further analysis, whereas particles outside of the fluorescence and light-scattering (side-scattered light [SSC]) gates were excluded (colored black and blue, respectively). Plots of the fluorescence and light-scattering properties of vesicles before (i and ii) and after (iii and iv) sorting show that particles falling within established gates were physically isolated; compare the tight grouping of the FAVS-purified LVs (iii and iv) with the wide dispersion of unsorted vesicles (i and ii). (C) Box and whisker plot of vesicle diameters measured from negative-stain TEM micrographs. The diameters of vesicles before (n = 1219) and after (n = 372) FAVS were measured from electron micrographs of negatively stained samples. Postsort vesicles displayed less variability in their size with no vesicles >170 nm, which is in contrast with the presort vesicles that regularly possessed membrane particles as large as 400 nm. (D) Samples of brush borders (BB) and pre- and post-FAVS–purified LVs were analyzed by Western blotting (loaded for equal total protein). FAVS-purified LVs show a clear enrichment in IAP when detected using either a polyclonal (IAP_P) or monoclonal (IAP_M) antibody. DPPIV, SI, and LPH are found at lower levels in LVs than in the brush border but all show modest enrichment after FAVS purification.

and detergent-soluble membrane fractions (Fig. 4 D). Although LVs contained many of the same proteins as microvillar membrane, they were depleted in SI, LPH, and MGAM. In contrast, LVs were enriched in a prominent doublet running between 50 and 100 kD in the lowest density fraction (Fig. 4 D, fraction 1). To identify these two major components, we excised both bands, trypsinized the samples, and performed liquid chromatography/mass spectrometry (MS) on the resulting peptides. Our results show with high confidence that these bands represent the two distinct forms of IAP expressed in the rat gastrointestinal tract (51% coverage of IAP1 and 30% coverage for IAP2; Xie and Alpers, 2000). Western blot analysis and enzyme activity assays confirmed that IAP is significantly enriched in the LV fraction compared with microvillar membranes (Fig. 4, C and D). Thus, although LVs and microvillar membranes share several common components, these data indicate that IAP is a principal cargo of LVs.

Because LVs are highly enriched in IAP (Fig. 4 D), one might expect to find that IAP is also enriched in the aforementioned distal tip membrane bulbs (Fig. 1). Indeed, small intestine frozen sections labeled with an antibody directed against IAP show intense labeling at the distal microvillus tips (Fig. 4 E). Consistent with the Western blot (Fig. 4 D) results, the type II transmembrane protein SI was also present in microvillar

membrane bulbs but did not exhibit the enrichment observed for IAP (Fig. 4 E). The enrichment of IAP at microvillar tips (Fig. 4 E) is consistent with the hypothesis that IAP-enriched LVs isolated from the intestinal lumen (Fig. 2) are derived from the enterocyte brush border.

IAP-enriched LVs are derived from enterocyte microvillar membrane

The morphological heterogeneity of vesicles in the LV fraction (Fig. 2 B) suggests that this material may represent a mixture of membranes from multiple cellular sources. However, we were interested in determining whether LVs enriched in IAP were derived specifically from enterocyte microvilli. To this end, we used a novel high performance flow cytometry approach called fluorescence-activated vesicle sorting (FAVS) to isolate only IAP-enriched vesicles (Cao et al., 2008). Our goal was to create a purified pool of IAP-enriched vesicles that could serve as input for proteomic analysis; the resulting dataset would provide definitive information on the origin of LVs. Vesicles in fraction 3 (Fig. 2) were labeled with the fluorescent lipophilic dye DiD (1,1'-dioctadecyl-3,3,3′,3′-tetramethylindodicarbocyanine perchlorate) and a polyclonal antibody directed against IAP (Sigma-Aldrich; detected with an Alexa Fluor 488–conjugated secondary antibody). By comparing the light-scattering and fluorescence signal characteristics of LVs with those of reference beads, we were able to isolate particles that were (a) double positive for both DiD and IAP, (b) single vesicles (i.e., not aggregates), and (c) in the expected size range of ∼100 nm (Fig. 5; see Materials and methods). Our ability to isolate particles meeting these criteria was confirmed by postsorting flow analysis (Fig. 5 B; note the wide dispersion of the input material relative to the tight grouping of the postsort particles within the established gates). Selection of particles of the appropriate size and composition was validated by negative-stain TEM and Western blot analysis (Fig. 5). Sorted vesicles had a slightly larger mean diameter (∼90 nm) and fell within a range of 30–170 nm, completely lacking the large (>400-nm diameter) particles observed in the input material (Fig. 5). Additionally, postsort LVs were highly enriched in IAP (the sorting marker) and modestly enriched in other microvillar membrane proteins such as SI, DPPIV, and LPH (Fig. 5 D). The uniform appearance of vesicles and accompanying enrichment in microvillar membrane markers confirmed the utility of FAVS for purifying IAP-enriched LVs.

After validating the FAVS purification procedure, sorted LVs were concentrated by ultracentrifugation and subjected to proteomic analysis. Peptide spectra were analyzed and assigned to protein identifications using MyriMatch software (Tabb et al., 2007); general characterization based on function and localization of identified proteins was determined using WebGestalt (version 2.0; http://bioinfo.vanderbilt.edu/wg2/; Zhang et al., 2005) and manually cross-checked against the National Center for Biotechnology Information database (http://www.ncbi.nlm.nih.gov/sites/entrez?db=Protein). Strikingly, several of the identified LV cargos are only expressed in enterocytes where they are known to localize to the microvillus; these include the actin-bundling protein ezrin, the carbohydrate-binding protein galectin-4, and a variety of well-characterized brush border hydrolases (Table I). Hydrolases made up the largest class of cargos and included peptidases, glycosidases, lipases, and phosphatases (Table I). LVs also contained several proteins that have been implicated in immunological function, inflammatory response, or are misregulated in cancer; prominent examples include the polymeric Ig receptor (Murthy et al., 2006), several annexins (Gerke et al., 2005), meprin (Lottaz et al., 2007), syncollin (Tan and Hooi, 2000), alkaline sphingomyelinase (Hertervig et al., 1997; Sakata et al., 2007), and ceramidase (Teichgraber et al., 2008). Additional LV cargoes included proteins with established roles in modifying the chemistry or curvature of cellular membranes such as annexin A13b (Gerke et al., 2005) and secreted PLA2 (Table S1; Staneva et al., 2004). The identification of numerous membrane proteins that are components specifically found in the enterocyte brush border clearly shows that IAP-enriched vesicles are derived from the microvillar membrane.

Myo1a KO mice demonstrate defects in IAP-enriched LV production

Given that our structural, biochemical, and proteomic data all indicate that LVs are released from brush border microvilli, we sought to determine whether LV production was disrupted in the absence of the major microvillar motor protein, myo1a. Myo1a is likely to play a role in LV production in vivo, as our previous experiments have revealed that this motor is required to power the release of vesicles from microvillar tips in isolated brush borders (McConnell and Tyska, 2007). When KO lumen washes were processed to isolate LVs, we were surprised to find that even in the absence of myo1a, a significant amount of membranous material was present in the LV fraction. However, when we examined this material by negative-stain TEM, we observed that KO vesicles are significantly larger than those isolated from wild-type (WT) controls (Fig. 6 and Fig. S1). An increase in vesicle size was confirmed using analytical flow cytometry (vesicles labeled as in the aforementioned FAVS purification protocol) in which DiD fluorescence provides a readout on the relative amount of membrane present in each particle. Of the 10,000 WT LVs analyzed, we observed a nearly linear relationship between IAP content and vesicle size (DiD signal) with >92% of the vesicles grouping into a tightly defined gate (Fig. 6 B, blue). However, when KO LVs were processed identically, we found that nearly half of the KO vesicles fell outside of this area (48%; Fig. 6 B, red). This analysis reveals that KO vesicles contain more lipid (per particle) on average relative to WT (i.e., KO LVs are larger) and further suggests that the IAP/lipid ratio is lower than normal in the absence of myo1a.

To further characterize defects in the production of myo1a KO LVs, we analyzed the density of WT and KO vesicles in 100,000 *g* lumen wash pellets using self-forming Optiprep density gradients. With this approach, WT vesicles typically demonstrated peak IAP enrichment in the first gradient fraction (lowest density, ∼1.05 g/ml); KO samples lacked the enrichment of IAP in the first fraction, instead displaying an even distribution across the entire gradient (Fig. 7 A). These results are consistent with the aforementioned flow cytometry data described; both assays suggest that the effective

Table I. **IAP-enriched LVs contain markers of the enterocyte brush border membrane**

IPI accession no.	Coverage	Protein name	Links to intestinal pathophysiology
	%		
IPI00326462.1	36	Alkaline phosphodiesterase	Sjoqvist et al., 2002
IPI00230862.7	44	Aminopeptidase N	Rahbar et al., 2006
IPI00366259.3	64	Annexin A13b	ND
IPI00358059.2	24	Aspartyl aminopeptidase	ND
IPI00327713.1	16	Carboxypeptidase A1	ND
IPI00882402.1	8	CD82 antigen	Rahbar et al., 2006
IPI00195627.1	42	CLCA3/Gob5	Long et al., 2006
IPI00392472.2	12	CLCA4	Ritzka et al., 2004
IPI00417388.1	7	Choline transporter 4	ND
IPI00480639.3	8	Complement C3	Laufer et al., 2000
IPI00195931.1	30	D6.1A protein	Kuhn et al., 2007
IPI00327697.4	45	Dipeptidase 1	McIver et al., 2004
IPI00777229.1	18	DPPIV	ND
IPI00470254.4	6	Ezrin	Simpson et al., 2006
IPI00211324.1	23	Galectin-4	Paclik et al., 2008
IPI00327398.1	39	Glutamyl aminopeptidase	ND
IPI00781546.1	25	IgG Fc-binding protein	Kobayashi et al., 2002
IPI00196395.1[a]	55	IAP	Bates et al., 2007; Goldberg et al., 2008
IPI00767004.1	14	Intestinal alkaline sphingomyelinase	Soo et al., 2008
IPI00764148.1	15	LPH	Grand et al., 2003
IPI00193894.4	39	MGAM	ND
IPI00197684.1	28	Membrane-bound aminopeptidase P	ND
IPI00210872.5	9	Meprin A subunit α	Lottaz et al., 2007
IPI00204808.5	21	Meprin A subunit β	ND
IPI00551567.1	17	Major histocompactability complex class I RT1-Au heavy chain	ND
IPI00212316.1	8	Microsomal triglyceride transfer protein	Slight et al., 2004
IPI00208856.1	33	Mucin-13	ND
IPI00197154.1	31	NAALADase 1	ND
IPI00231789.5	38	Neprilysin	Barbara et al., 2003
IPI00211648.1	11	rBAT	ND
IPI00208165.1	13	Neutral ceramidase	Hertervig et al., 1997
IPI00776761.1	10	Phospholipid scramblase 1	ND
IPI00231197.6	11	Platelet glycoprotein 4	Hoebe et al., 2005
IPI00205255.1	18	Polymeric immunoglobulin receptor	Sano et al., 2008
IPI00191437.4	38	SI	Ryu et al., 2001
IPI00212367.1	22	Syncollin	Tan and Hooi, 2000
IPI00200117.1	17	Syntenin-1	Chen et al., 2008
IPI00199458.1	3	Tetraspanin 1	ND
IPI00366513.3	18	Trehalase	Arvanitakis, 1979

IPI, International Protein Index.
[a]Significant finding of this study.

IAP concentration in KO vesicles is reduced. To determine whether vesicle composition was altered in general, WT and KO vesicles from sucrose gradient fraction 3 were analyzed by Western blotting (loaded for equal total protein). We found that although IAP levels appear comparable, KO LVs possess abnormally high levels of other brush border membrane proteins such as MGAM, SI, and LPH when compared with WT (Fig. 7 B). Intriguingly, we observed a corresponding decrease in the levels of these enzymes in KO brush borders (Fig. 7 B). When the disaccharidase activities of equivalent amounts of LVs and brush borders were compared (equal total protein), we observed that both sucrase and maltase activities were high in WT brush borders with minimal activity present in WT LVs. However, KO LVs showed high disaccharidase activities with a corresponding decrease in these activities in KO brush borders (Fig. 7 C).

Given the high expression level of myo1a in the enterocyte and its specific targeting to microvilli, the data derived from experiments with myo1a KO mice provide strong evidence implicating the microvillus as the source of LVs. Moreover, the redistribution of components from the brush border into LVs in KO animals indicates that myo1a is critical for the production of vesicles that contain a normal complement of enzymes and are specifically enriched in IAP.

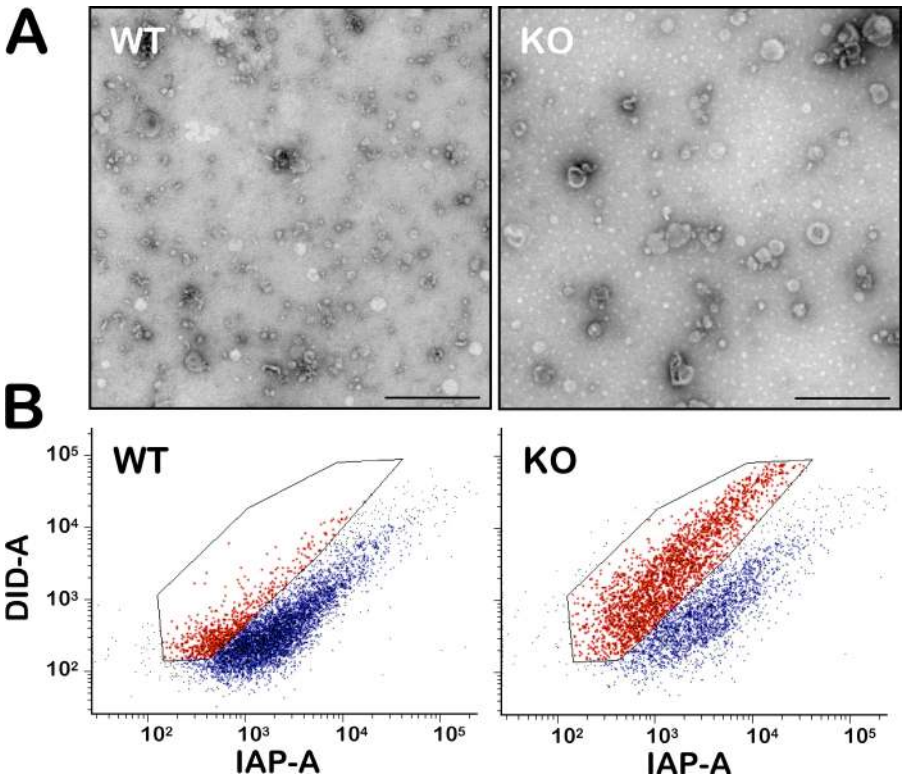

Figure 6. **LVs isolated from myo1a KO mice exhibit abnormal morphology.** (A) Negative-stain TEM clearly shows that LVs isolated from myo1a KO mice are much larger than WT controls. Bars, 0.5 µm. (B) Flow cytometric analysis of WT and KO LVs fluorescently labeled with the membrane dye DiD and an antibody directed against IAP. KO LVs had much higher DiD fluorescence per particle, suggesting that these particles had more membrane; i.e., vesicles are larger. This larger size is clearly visualized by the shift up the y axis; compare the outlined areas in WT and KO (included particles highlighted in red). Although only 12% of WT particles fall into this gate, nearly half (48%) of the particles analyzed from KO mice demonstrated increased DiD fluorescence. 10,000 particles were analyzed for each condition.

Discussion

Enterocyte microvilli function as vesicle-generating organelles

Previous studies have reported the presence of vesicles in the intestinal lumen (Eliakim et al., 1989; Beaudoin and Grondin, 1991; Halbhuber et al., 1994), although their function, origin, and mechanism of formation have not been elucidated. These studies, in combination with recent in vitro studies conducted in our laboratory (McConnell and Tyska, 2007), led us to hypothesize that enterocyte microvilli could serve as the source of these membranes by releasing vesicles laden with brush border enzymes from their distal tips. In this study, we present multiple lines of evidence in support of this model: (a) morphological experiments of native enterocytes clearly show that apical membrane forms bulbous protrusions at microvillar tips, (b) EM and biochemical analysis of intestinal lumen wash reveals that this material contains vesicles with the expected diameter and orientation (~90 nm; right side out) for membranes released from microvillar tips, (c) LVs and membrane bulbs at the tips of microvilli are specifically enriched in IAP, (d) proteomic analysis of purified, flow-sorted LVs confirms that these vesicles contain an array of catalytically active enzymes (IAP, SI, MGAM, and aminopeptidase N) that are specific markers for the enterocyte microvillar membrane, and (e) the absence of myo1a causes defects in the structure and composition of both the enterocyte brush border (Tyska et al., 2005) and LVs (Figs. 6 and 7). Together, these data indicate that microvilli play a role beyond that of passively scaffolding apical membrane by functioning as active vesicle-generating organelles.

Myo1a is required for proper LV production

Within the intestinal tract, myo1a is expressed only in enterocytes and localizes exclusively to brush border microvilli (Bikle et al., 1991). Thus, the abnormal LVs isolated from myo1a KO mice provide strong evidence indicating that these membranes are microvillus derived. The vesicles isolated from KO mice could be produced in one of two ways: (1) actively, by myosin motors that redistribute into the brush border in the absence of myo1a or (2) passively, perhaps via mechanical shearing of large membrane herniations from the apical surfaces of KO enterocytes (Tyska et al., 2005). This type of unregulated membrane loss could explain the increased variability observed in vesicle size (Fig. 6) and density (Fig. 7 A) as well as the increased amounts of proteins such as SI, LPH, and MGAM that are normally excluded from LVs and retained in the microvillar membrane (Fig. 7, B and C).

The precise role of myo1a-derived forces in the formation of LVs and their subsequent release from microvillar tips remains unclear. However, it is possible that mechanical forces exerted on the membrane along the microvillar axis may provide a physical stimulus that leads to the fission of membrane from microvillar tips (Hobbs, 1980). Alternatively, myo1a might play a role in the sorting of specific high curvature lipids or other fission machinery into the tip compartment, a possibility discussed in more detail in the following section. Elucidating the details of how myo1a contributes to the formation and release of LVs will likely become the focus of future studies.

Enrichment of IAP at the microvillus tip

Actin-based cellular protrusions have been shown to enrich transmembrane proteins at their distal tips to carry out specialized

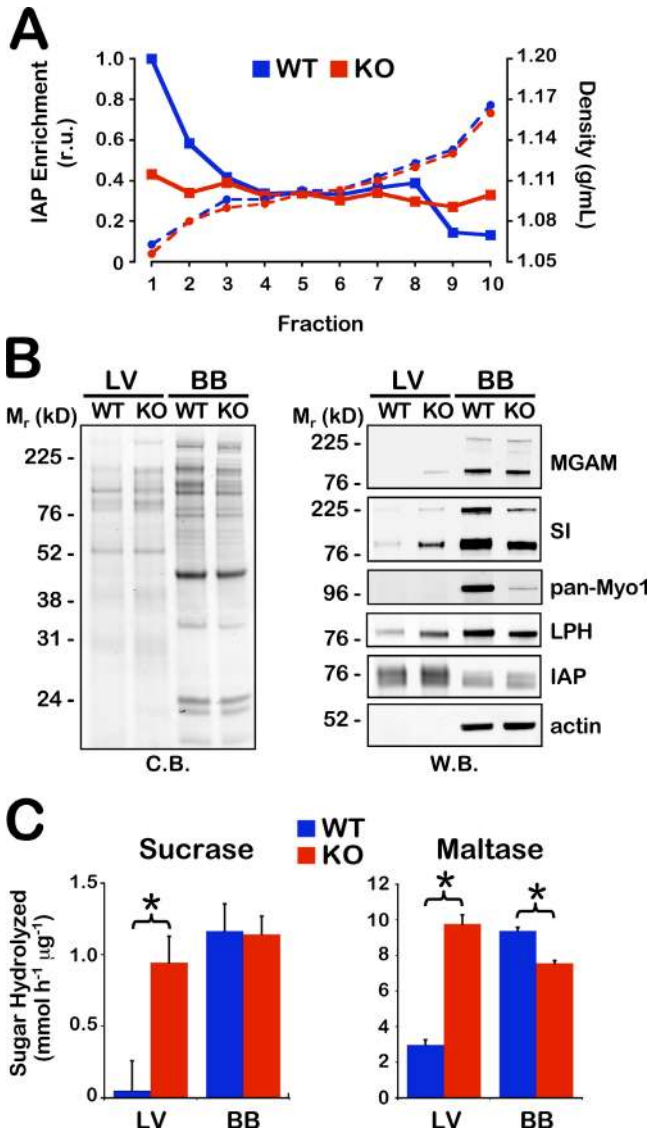

Figure 7. **LVs isolated from myo1a KO mice exhibit defects in protein composition.** (A) To analyze LV density, lumen wash material from WT and KO mice was fractionated by differential centrifugation as described in Materials and methods. The 100,000 *g* pellets were resuspended in PBS, loaded onto 20% self-forming Optiprep gradients, and centrifuged at 200,000 *g* for 2 h. Gradients were split into 10 equal-volume fractions; dashed lines denote fraction density. WT LVs demonstrate clear enrichment of IAP in low density fractions (fractions 1 and 2); this enrichment is completely lacking in the KO LVs. IAP enrichment was calculated by normalizing IAP levels (Western blot densitometry) against total protein for each fraction. (B) Polyacrylamide gel of LV and brush border (BB) samples isolated from WT and myo1a KO mice stained with Coomassie blue (CB). The increased staining in the KO LV sample in the high molecular mass range (76–225 kD) was observed in multiple experiments. When these samples were analyzed by Western blotting (WB) using antibodies directed against brush border membrane proteins found in this size range, we observed that several integral membrane proteins normally found at low levels in WT LVs are present at significantly higher levels in KO LVs (e.g., MGAM, SI, and LPH). (C) Sucrase and maltase activities of LV and brush border samples isolated from WT and KO mice were assayed by measuring glucose liberated from sucrose and maltose, respectively (12.5 µg protein per condition). Both sucrase and maltase activities distributed differently, with KO LVs showing higher disaccharidase activities than WT LVs, whereas KO brush borders showed a corresponding decrease in these activities relative to WT brush borders. Values are given as millimoles of sugar hydrolyzed per hour per microgram of protein (mmol h^{-1} µg^{-1}). Sucrase: WT LV, 0.05 ± 0.21; KO LV, 0.94 ± 0.18; WT brush border, 1.16 ± 0.19; KO brush border, 1.14 ± 0.13. Maltase: WT LV, 2.97 ± 0.29; KO LV, 9.76 ± 0.52; WT brush border, 9.4 ± 0.19; KO brush border, 7.55 ± 0.15. Conditions were considered statistically significant if $P < 0.05$ (denoted by an asterisk).

functions such as mechano-sensitive ion gating in the case of stereocilia (Hudspeth and Gillespie, 1994) or integrin-mediated cellular adhesion in the case of filopodia (Zhang et al., 2004). Although microvilli are a classical model for studying organized actin arrays (Mooseker and Tilney, 1975), little is known about the distribution of membrane or cytoskeletal components along the microvillar axis. The first protein to be localized to the microvillus tip was the actin-regulating protein Eps8 (Croce et al., 2004). Another recent study has shown that ezrin and the ezrin-interacting protein EPI64 localize in a gradient with highest levels at the microvillar tip (Hanono et al., 2006). To our knowledge, the IAP enrichment described in this study is the first demonstration of microvillus tip localization for a membrane protein.

An interesting question arises as to the mechanism that may drive the polarized localization of IAP. Transmembrane proteins that localize to the tips of stereocilia and filopodia are transported to the protrusion's distal end by myosin motor proteins (Tokuo and Ikebe, 2004; Delprat et al., 2005). However, because IAP is localized to the extracellular leaflet of the plasma membrane by a glycosylphosphatidylinositol linkage, it does not have direct access to motor proteins that might provide plus end–directed transport. Viewed from an alternate perspective, lack of tethering to the underlying cytoskeleton might be important for allowing the "flow" of IAP along the microvillar axis and into the tip compartment; molecules that are tethered to the actin core may be prevented from flowing toward the distal tip. We postulate that tipward flow of untethered membrane components could be driven by the biosynthetic delivery of material to the base of microvilli and release of vesicles from microvillar tips. This hypothesis is consistent with a previous study, which established that SI, a type II transmembrane protein, interacts directly with myo1a and that this interaction is required to retain SI in the brush border (Tyska and Mooseker, 2004). This idea also finds support in the biochemical and immunofluorescence data presented in this study, which reveal that although LVs contain SI, levels are low compared with brush border membranes (Fig. 4). Moreover, in the absence of myo1a, SI levels in the brush border decrease, whereas more of this transmembrane protein is found in LVs (Fig. 7). In combination, these data support a model in which differential tethering to the actin core via motors such as myo1a plays an important role in producing the enrichment of specific components (e.g., IAP) at microvillar tips.

Mechanism of LV formation and release from microvillar tips

A key goal for future studies will be to investigate the mechanistic details of LV formation and release from microvillar tips as well as the regulation of this process by physiological and pathophysiological stimuli. Clues to the machinery involved in this process may be found in the LV proteome described in

this study (Table I). FAVS-purified LVs contain several proteins that are expressed at high levels in the enterocyte brush border (Table I). Among these are several lipid-binding proteins, including eight members of the annexin family (A1-5, A7, A11, and A13b) and secreted PLA2 (Table S1). These components are of particular interest because annexins are involved in mediating actin–membrane interactions (Merrifield et al., 2001; Hayes et al., 2004) during several membrane fission and fusion events (Gerke et al., 2005) and thus may play a key role in the formation or release of LVs from the actin-rich microvillus. PLA2 hydrolyzes phospholipids into arachidonic acid and lysophospholipids and thus plays a key role in the generation of proinflammatory second messengers such as prostaglandins and leukotrienes (Dennis et al., 1991). Because it removes the *sn*-2 acyl chain of phospholipids, PLA2 activity also changes membrane curvature, which has been shown to cause the spontaneous fission and vesiculation of lipid rafts from liposomes in vitro (Staneva et al., 2004). This is of particular interest, as both the microvillar membrane and LVs are enriched in proteins that preferentially partition into lipid rafts such as IAP.

Physiological function of microvillar membrane shedding

The release of vesicles laden with catalytically active hydrolases could allow processing of target substrates to take place without the need for substrate to be in direct contact with the enterocyte apical surface (Jacobs, 1983). Although previous ultrastructural studies described the presence of such vesicles in the intestinal lumen (DeSchryver-Kecskemeti et al., 1989; Halbhuber et al., 1994), the cellular origin of these vesicles remained unclear. Interestingly, compositional differences between vesicles and the enterocyte plasma membrane were originally interpreted as evidence that the vesicles were not derived from the brush border (DeSchryver-Kecskemeti et al., 1989). However, the enrichment of specific enzymes at sites of vesicle release, such as IAP enrichment at microvillar tips (Fig. 4 E), would explain this apparent discrepancy.

The enrichment of IAP in LVs suggests that a primary function of these vesicles is the distribution of phosphatase activity throughout the intestinal lumen. Although the precise role of IAP in the gastrointestinal tract was unknown for many years, recent work in mouse and zebrafish model systems now shows that IAP is a vital component of the mucosal barrier (Beumer et al., 2003; van Veen et al., 2005; Su et al., 2006; Bates et al., 2007; Goldberg et al., 2008). Specifically, IAP is able to dephosphorylate and thus detoxify bacterial lipopolysaccharide (LPS). An abundant component of the gram-negative bacterial outer membrane, LPS is a potent and highly concentrated proinflammatory ligand in the gastrointestinal tract; dephosphorylation of the lipid A moiety of LPS reduces the toxicity of this compound at least 100-fold (Schromm et al., 1998). The production of IAP-enriched LVs could be a mechanism that enterocytes use to detoxify LPS in the intestinal lumen in an effort to minimize its proinflammatory impact on cells of the mucosa.

Concluding remarks

Microvillar membrane shedding represents a novel aspect of epithelial cell biology that may provide the enterocyte with a means for catalytically conditioning the lumenal environment. Given that LVs are specifically enriched in IAP activity, which may be involved in host defense against gram-negative bacteria, these vesicles may play an important role in mucosal barrier function. The work presented in this study provides a critical first step toward understanding the role of this new aspect of enterocyte function. Future studies will attempt to illuminate the molecular mechanisms governing LV function and seek to identify physiological stimuli that may regulate LV release.

Materials and methods

Light microscopy

All procedures involving animals were undertaken following approval from the Vanderbilt University Medical Center Institutional Animal Care and Use Committee. All reagents were obtained from Sigma-Aldrich unless noted otherwise. Small intestines from WT 129 SVJ1 mice were collected, flushed with warm HBSS (Invitrogen), cut into 10-cm lengths, filled with 4% PFA, and the ends were clamped and fixed at room temperature for 10 min. Intestine segments were opened longitudinally, rolled, fixed in 4% PFA for 1 h on ice, and incubated in 1 M sucrose in TBS (150 mM NaCl and 50 mM Tris, pH 8.0) overnight at 4°C. Tissue was embedded in OCT, frozen, and 20-µm-thick transverse sections were cut on a cryostat (Leica). Sections were stained using Alexa Fluor 488–Con A (1:200; Invitrogen), phalloidin conjugated to either Alexa Fluor 568 or 633 (1:200; Invitrogen), anti-IAP (1:200; Sigma-Aldrich), and Alexa Fluor 568 secondary antibody (1:200; Invitrogen). Micrographs were acquired using a laser-scanning confocal microscope with a 100×/1.4 NA Plan Apo objective (FV-1000; Olympus). Images were pseudocolored, contrast enhanced, and cropped using ImageJ software (version 1.42i; National Institutes of Health).

LV isolation

For each LV preparation, adult Sprague-Dawley rats or adult 129 SVJ1 mice (WT and/or myo1a KO) were sacrificed and their intestines removed into ice-cold saline (150 mM NaCl, 2 mM imidazole-Cl, and 0.02% Na-Azide). The intestinal contents were collected by flushing each intestine with 30–60 ml cold saline into a beaker. The flushed material was put through a series of centrifugation steps, with the supernatant from the preceding spin loaded into the subsequent spin: 500 *g* for 20 min (SX4750 rotor; Beckman Coulter), 20,000 *g* for 30 min (SS34 rotor; Sorvall), and 100,000 *g* for 2 h (70Ti rotor; Beckman Coulter). The 100,000 *g* pellet was resuspended in PBS (137 mM NaCl, 7 mM Na_2HPO_4, and 3 mM NaH_2PO_4, pH 7.2), layered on top of a sucrose step gradient (equal volumes of 55, 38, 35, 25, 16, and 8% sucrose in PBS), and centrifuged at 100,000 *g* for 16 h in a swinging-bucket rotor (TH641; Sorvall). The gradient was split into equal volume fractions; to remove sucrose, each fraction was diluted with 10 vol PBS and centrifuged at 100,000 *g* for 2 h (70.1Ti rotor; Beckman Coulter), and the resulting pellets were resuspended in PBS.

EM

All EM reagents were purchased from EMS. For SEM, specimens were washed several times in warm HBSS and fixed overnight at 4°C with 3% glutaraldehyde in SEM buffer (0.1 M sucrose and 0.1 M Na-phosphate, pH 7.4). Samples were washed in SEM buffer, postfixed with 1% OsO_4 on ice for 1 h, and washed in SEM buffer. Samples were dehydrated in a graded ethanol series, dried with hexamethyldisilazane, mounted on aluminum stubs, coated with gold in a sputter coater, and viewed on a microscope (S-4200; Hitachi). For negative-stain TEM, LVs were deposited on glow-discharged formvar carbon grids and stained with 1% uranyl acetate. For thin section TEM, LVs were fixed with 3% glutaraldehyde overnight at 4°C, postfixed with 1% OsO_4 on ice for 2 h, washed with water, stained overnight in 1% uranyl acetate, dehydrated in a graded ethanol series, embedded in Embed812 according to the manufacturer's protocols (EMS), and sections were cut using an ultramicrotome (Leica). All grids were imaged on a transmission electron microscope (CM12; Phillips) equipped with an 8-bit grayscale charge-coupled device camera (Hamamatsu Photonics). Images were contrast enhanced and cropped using ImageJ software.

SDS-PAGE and immunoblotting

Protein fractions were analyzed with SDS-PAGE using 4–12% NuPage gradient gels. For immunoblotting, gels were transferred to nitrocellulose

membranes. Stock solutions of primary antibodies were diluted 1:1,000 before use and detected with Alexa Fluor 680– or 800–conjugated secondary antibodies (1:10,000) and imaged using a scanner (Odyssey; LI-COR Biosciences). Primary antibodies used in this study include anti-SI, anti-LPH, anti-DPPIV, anti-MGAM (provided by B. Nichols, Baylor College of Medicine, Houston, TX), anti-IAP (Sigma-Aldrich), antiactin (Sigma-Aldrich), and a pan-myo1 monoclonal antibody (Carboni et al., 1988).

Enzyme activity assays

To measure enzyme activity, the LV fraction was resuspended in TBS supplemented with 1 mM $MgCl_2$. Protein content was determined using a Bradford protein assay. For each reaction, 100 µg of the LV fraction protein was mixed with a range of substrate concentrations in 0.2 ml TBS and incubated at 37°C for 30 min. All assays were measured using a microplate reader (Synergy HT; Biotek). To measure alkaline phosphatase and aminopeptidase activities, the quenched fluorescent substrates 4-methylumbelliferyl phosphate and *H*-Leu-7-amino-4-methylcoumarin (MP Biomedicals) were used, respectively, and fluorescence at 460 nm was measured using 360-nm excitation. Disaccharidase activities were measured by incubating 25 µg LVs or isolated brush borders with sucrose or maltose, and the released glucose was quantified using a glucose hexokinase assay (Sigma-Aldrich).

LV purification by FAVS

For FAVS analysis, LVs were labeled using the following procedure: LVs were blocked for 1 h at 4°C with 2% bovine serum albumin, labeled with anti-IAP antibody (1:400; Sigma-Aldrich) and DiD (1:400; Invitrogen) for 1 h at 4°C, pelleted (100,000 *g* for 1 h; TLA 120.2 rotor; Beckman Coulter), washed in PBS, pelleted again, resuspended in PBS, and Alexa Fluor 488–conjugated goat anti–rabbit secondary antibody was added (1:400) for 1 h at 4°C (Invitrogen). LVs were pelleted, washed, resuspended in PBS, and sheared through a 27-gauge needle six times to dissociate vesicle aggregates. FAVS was performed as previously described (Cao et al., 2008). In brief, sorting was performed using an FACSAria (BD) equipped with forward scatter photomultiplier tubes; linearity and sensitivity were checked using eight-peak beads (Spherotech). Particle size resolution was determined using green fluorescent beads covering the size range of 40–700 nm (Duke Scientific). A custom high salt sheath fluid (78 mM KCl, 4 mM $MgCl_2$, 8 mM $CaCl_2$, 10 mM EGTA, and 50 mM Hepes-KOH, pH 7.0) was filtered through a 100-nm filter before loading into the Aria sheath reservoir. Two 200-nm in-line filters were used to assure low sheath background. Unstained and single-stained (anti-IAP or DiD only) vesicles were used to compensate spectral overlap, which was minimal. Double-stained vesicles were gated and pulse processed to detect doublet vesicles, and individual double-positive LVs were gated to remove vesicles >0.55 SD from their mean fluorescent intensities.

MS analysis of FAVS-purified LVs

FAVS-purified LVs were loaded onto 10% polyacrylamide gels and samples run into the gel ~1–2 cm. The gel was stained with Coomassie colloidal blue (Bio-Rad Laboratories) to visualize protein, and the entire protein-rich band at the top of the gel was excised, minced, and treated with trypsin to generate peptides for mass analysis. Liquid chromatography/MS/MS analysis of the resulting peptides was performed using an ion-trap mass spectrometer (Thermo Finnigan LTQ; Thermo Fisher Scientific) equipped with an autosampler (MicroAS; Thermo Fisher Scientific) and an HPLC pump (Surveyor; Thermo Fisher Scientific), nanospray source, and Xcalibur (version 1.4; Thermo Fisher Scientific) instrument control. Samples were subjected to a reverse-phase separation directly in line with the aforementioned LTQ. The MS/MS spectra of the peptides were performed using data-dependent scanning in which one full MS spectrum was followed by three MS/MS spectra. Peptide spectra were assigned to protein identifications using MyriMatch software (Tabb et al., 2007).

Statistical analysis

A Student's *t* test was used to analyze the data presented in Figs. 3 and 7. $P < 0.05$ was considered statistically significant.

Online supplemental material

Fig. S1 shows a histogram analysis of WT and myo1a KO LV size distributions observed by negative-stain TEM. Table S1 shows a complete list of proteins detected in LVs by MS. Online supplemental material is available at http://www.jcb.org/cgi/content/full/jcb.200902147/DC1.

We would like to thank Buford Nichols for the generous gift of several antibodies, Chin Chiang (Vanderbilt University Medical Center [VUMC]) for use of his cryostat, James Goldenring (VUMC) for valuable advice, Bing Zhang (VUMC) for use of WebGestalt software, Denny Kerns and the VUMC Cell Imaging Shared Resource, the Vanderbilt Mass Spectrometry Research Center, and members of the Tyska laboratory for their enthusiasm during vesicle collection.

This work was supported in part by the VUMC Training Program in Developmental Biology (HD07502), an American Heart Association predoctoral fellowship (to R.E. McConnell), and grants from the National Institutes of Health (DK-075555 to M.J. Tyska, CA-46413 to R.J. Coffey, CA-126218 to D.L. Tabb, Special Program of Research Excellence grant NCI P50 95103, Mouse Models of Human Cancers Consortium grant U01 084239, and Vanderbilt Digestive Diseases Research Core grant P30 DK-058404).

Submitted: 27 February 2009
Accepted: 3 June 2009

References

Arvanitakis, C. 1979. Abnormalities of jejunal mucosal enzymes in ulcerative colitis and Crohn's disease. *Digestion.* 19:259–266.

Bailey, D.S., A.R. Freedman, S.C. Price, D. Chescoe, and P.J. Ciclitira. 1989. Early biochemical responses of the small intestine of coeliac patients to wheat gluten. *Gut.* 30:78–85.

Barbara, G., R. De Giorgio, V. Stanghellini, R. Corinaldesi, C. Cremon, N. Gerard, C. Gerard, E.F. Grady, N.W. Bunnett, P.A. Blennerhassett, and S.M. Collins. 2003. Neutral endopeptidase (EC 3.4.24.11) downregulates the onset of intestinal inflammation in the nematode infected mouse. *Gut.* 52:1457–1464.

Bates, J.M., J. Akerlund, E. Mittge, and K. Guillemin. 2007. Intestinal alkaline phosphatase detoxifies lipopolysaccharide and prevents inflammation in zebrafish in response to the gut microbiota. *Cell Host Microbe.* 2:371–382.

Beaudoin, A.R., and G. Grondin. 1991. Shedding of vesicular material from the cell surface of eukaryotic cells: different cellular phenomena. *Biochim. Biophys. Acta.* 1071:203–219.

Beumer, C., M. Wulferink, W. Raaben, D. Fiechter, R. Brands, and W. Seinen. 2003. Calf intestinal alkaline phosphatase, a novel therapeutic drug for lipopolysaccharide (LPS)-mediated diseases, attenuates LPS toxicity in mice and piglets. *J. Pharmacol. Exp. Ther.* 307:737–744.

Bikle, D.D., S. Munson, and M.L. Mancianti. 1991. Limited tissue distribution of the intestinal brush border myosin I protein. *Gastroenterology.* 100:395–402.

Brown, A.L. Jr. 1962. Microvilli of the human jejunal epithelial cell. *J. Cell Biol.* 12:623–627.

Cao, Z., C. Li, J.N. Higginbotham, J.L. Franklin, D.L. Tabb, R. Graves-Deal, S. Hill, K. Cheek, W.G. Jerome, L.A. Lapierre, et al. 2008. Use of fluorescence-activated vesicle sorting for isolation of Naked2-associated, basolaterally targeted exocytic vesicles for proteomics analysis. *Mol. Cell. Proteomics.* 7:1651–1667.

Carboni, J.M., K.A. Conzelman, R.A. Adams, D.A. Kaiser, T.D. Pollard, and M.S. Mooseker. 1988. Structural and immunological characterization of the myosin-like 110-kD subunit of the intestinal microvillar 110K-calmodulin complex: evidence for discrete myosin head and calmodulin-binding domains. *J. Cell Biol.* 107:1749–1757.

Chen, F., Y. Du, Z. Zhang, G. Chen, M. Zhang, H.B. Shu, Z. Zhai, and D. Chen. 2008. Syntenin negatively regulates TRAF6-mediated IL-1R/TLR4 signaling. *Cell. Signal.* 20:666–674.

Croce, A., G. Cassata, A. Disanza, M.C. Gagliani, C. Tacchetti, M.G. Malabarba, M.F. Carlier, G. Scita, R. Baumeister, and P.P. Di Fiore. 2004. A novel actin barbed-end-capping activity in EPS-8 regulates apical morphogenesis in intestinal cells of *Caenorhabditis elegans*. *Nat. Cell Biol.* 6:1173–1179.

Cutz, E., J.M. Rhoads, B. Drumm, P.M. Sherman, P.R. Durie, and G.G. Forstner. 1989. Microvillus inclusion disease: an inherited defect of brush-border assembly and differentiation. *N. Engl. J. Med.* 320:646–651.

Delprat, B., V. Michel, R. Goodyear, Y. Yamasaki, N. Michalski, A. El-Amraoui, I. Perfettini, P. Legrain, G. Richardson, J.P. Hardelin, and C. Petit. 2005. Myosin XVa and whirlin, two deafness gene products required for hair bundle growth, are located at the stereocilia tips and interact directly. *Hum. Mol. Genet.* 14:401–410.

Dennis, E.A., S.G. Rhee, M.M. Billah, and Y.A. Hannun. 1991. Role of phospholipase in generating lipid second messengers in signal transduction. *FASEB J.* 5:2068–2077.

DeSchryver-Kecskemeti, K., R. Eliakim, S. Carroll, W.F. Stenson, M.A. Moxley, and D.H. Alpers. 1989. Intestinal surfactant-like material. A novel secretory product of the rat enterocyte. *J. Clin. Invest.* 84:1355–1361.

Eliakim, R., K. DeSchryver-Kecskemeti, L. Nogee, W.F. Stenson, and D.H. Alpers. 1989. Isolation and characterization of a small intestinal surfactant-like particle containing alkaline phosphatase and other digestive enzymes. *J. Biol. Chem.* 264:20614–20619.

Gerke, V., C.E. Creutz, and S.E. Moss. 2005. Annexins: linking Ca2+ signalling to membrane dynamics. *Nat. Rev. Mol. Cell Biol.* 6:449–461.

Goldberg, R.F., W.G. Austen Jr., X. Zhang, G. Munene, G. Mostafa, S. Biswas, M. McCormack, K.R. Eberlin, J.T. Nguyen, H.S. Tatlidede, et al. 2008. Intestinal alkaline phosphatase is a gut mucosal defense factor maintained by enteral nutrition. *Proc. Natl. Acad. Sci. USA.* 105:3551–3556.

Grand, R.J., R.K. Montgomery, D.K. Chitkara, and J.N. Hirschhorn. 2003. Changing genes; losing lactase. *Gut.* 52:617–619.

Halbhuber, K.J., M. Schulze, H. Rhode, R. Bublitz, H. Feuerstein, M. Walter, W. Linss, H.W. Meyer, and A. Horn. 1994. Is the brush border membrane of the intestinal mucosa a generator of "chymosomes"? *Cell Mol. Biol. (Noisy-le-grand).* 40:1077–1096.

Hanono, A., D. Garbett, D. Reczek, D.N. Chambers, and A. Bretscher. 2006. EPI64 regulates microvillar subdomains and structure. *J. Cell Biol.* 175:803–813.

Hayes, M.J., U. Rescher, V. Gerke, and S.E. Moss. 2004. Annexin-actin interactions. *Traffic.* 5:571–576.

Hertervig, E., A. Nilsson, L. Nyberg, and R.D. Duan. 1997. Alkaline sphingomyelinase activity is decreased in human colorectal carcinoma. *Cancer.* 79:448–453.

Hobbs, D.G. 1980. The origin and distribution of membrane-bound vesicles associated with the brush border of chick intestinal mucosa. *J. Anat.* 131:635–642.

Hoebe, K., P. Georgel, S. Rutschmann, X. Du, S. Mudd, K. Crozat, S. Sovath, L. Shamel, T. Hartung, U. Zahringer, and B. Beutler. 2005. CD36 is a sensor of diacylglycerides. *Nature.* 433:523–527.

Hudspeth, A.J., and P.G. Gillespie. 1994. Pulling springs to tune transduction: adaptation by hair cells. *Neuron.* 12:1–9.

Iancu, T., and E. Elian. 1976. The intestinal microvillus. Ultrastructural variability in coeliac disease and cow's milk intolerance. *Acta Paediatr. Scand.* 65:65–73.

Jacobs, L.R. 1983. Biochemical and ultrastructural characterization of the molecular topography of the rat intestinal microvillous membrane. Asymmetric distribution of hydrophilic groups and anionic binding sites. *Gastroenterology.* 85:46–54.

Kobayashi, K., H. Ogata, M. Morikawa, S. Iijima, N. Harada, T. Yoshida, W.R. Brown, N. Inoue, Y. Hamada, H. Ishii, et al. 2002. Distribution and partial characterisation of IgG Fc binding protein in various mucin producing cells and body fluids. *Gut.* 51:169–176.

Kuhn, S., M. Koch, T. Nubel, M. Ladwein, D. Antolovic, P. Klingbeil, D. Hildebrand, G. Moldenhauer, L. Langbein, W.W. Franke, et al. 2007. A complex of EpCAM, claudin-7, CD44 variant isoforms, and tetraspanins promotes colorectal cancer progression. *Mol. Cancer Res.* 5:553–567.

Laufer, J., R. Oren, I. Goldberg, A. Horwitz, J. Kopolovic, Y. Chowers, and J.H. Passwell. 2000. Cellular localization of complement C3 and C4 transcripts in intestinal specimens from patients with Crohn's disease. *Clin. Exp. Immunol.* 120:30–37.

Long, A.J., J.P. Sypek, R. Askew, S.C. Fish, L.E. Mason, C.M. Williams, and S.J. Goldman. 2006. Gob-5 contributes to goblet cell hyperplasia and modulates pulmonary tissue inflammation. *Am. J. Respir. Cell Mol. Biol.* 35:357–365.

Loomis, P.A., L. Zheng, G. Sekerkova, B. Changyaleket, E. Mugnaini, and J.R. Bartles. 2003. Espin cross-links cause the elongation of microvillus-type parallel actin bundles in vivo. *J. Cell Biol.* 163:1045–1055.

Lottaz, D., C. Buri, G. Monteleone, S. Rosmann, T.T. Macdonald, I.R. Sanderson, and E.E. Sterchi. 2007. Compartmentalised expression of meprin in small intestinal mucosa: enhanced expression in lamina propria in coeliac disease. *Biol. Chem.* 388:337–341.

Maestracci, D. 1976. Enzymic solubilization of the human intestinal brush border membrane enzymes. *Biochim. Biophys. Acta.* 433:469–481.

McConnell, R.E., and M.J. Tyska. 2007. Myosin-1a powers the sliding of apical membrane along microvillar actin bundles. *J. Cell Biol.* 177:671–681.

McIver, C.M., J.M. Lloyd, P.J. Hewett, and J.E. Hardingham. 2004. Dipeptidase 1: a candidate tumor-specific molecular marker in colorectal carcinoma. *Cancer Lett.* 209:67–74.

Merrifield, C.J., U. Rescher, W. Almers, J. Proust, V. Gerke, A.S. Sechi, and S.E. Moss. 2001. Annexin 2 has an essential role in actin-based macropinocytic rocketing. *Curr. Biol.* 11:1136–1141.

Mooseker, M.S. 1985. Organization, chemistry, and assembly of the cytoskeletal apparatus of the intestinal brush border. *Annu. Rev. Cell Biol.* 1:209–241.

Mooseker, M.S., and L.G. Tilney. 1975. Organization of an actin filament-membrane complex. Filament polarity and membrane attachment in the microvilli of intestinal epithelial cells. *J. Cell Biol.* 67:725–743.

Mooseker, M.S., and T.R. Coleman. 1989. The 110-kD protein-calmodulin complex of the intestinal microvillus (brush border myosin I) is a mechanoenzyme. *J. Cell Biol.* 108:2395–2400.

Murthy, A.K., C.N. Dubose, J.A. Banas, J.J. Coalson, and B.P. Arulanandam. 2006. Contribution of polymeric immunoglobulin receptor to regulation of intestinal inflammation in dextran sulfate sodium-induced colitis. *J. Gastroenterol. Hepatol.* 21:1372–1380.

Paclik, D., S. Danese, U. Berndt, B. Wiedenmann, A. Dignass, and A. Sturm. 2008. Galectin-4 controls intestinal inflammation by selective regulation of peripheral and mucosal T cell apoptosis and cell cycle. *PLoS ONE.* 3:e2629.

Rahbar, A., L. Bostrom, and C. Soderberg-Naucler. 2006. Detection of cytotoxic CD13-specific autoantibodies in sera from patients with ulcerative colitis and Crohn's disease. *J. Autoimmun.* 26:155–164.

Revenu, C., R. Athman, S. Robine, and D. Louvard. 2004. The co-workers of actin filaments: from cell structures to signals. *Nat. Rev. Mol. Cell Biol.* 5:635–646.

Ritzka, M., F. Stanke, S. Jansen, A.D. Gruber, L. Pusch, S. Woelfl, H.J. Veeze, D.J. Halley, and B. Tummler. 2004. The CLCA gene locus as a modulator of the gastrointestinal basic defect in cystic fibrosis. *Hum. Genet.* 115:483–491.

Ryu, H., Y.S. Kim, P.A. Grange, and F.J. Cassels. 2001. *Escherichia coli* strain RDEC-1 AF/R1 endogenous fimbrial glycoconjugate receptor molecules in rabbit small intestine. *Infect. Immun.* 69:640–649.

Sakata, A., K. Yasuda, T. Ochiai, H. Shimeno, S. Hikishima, T. Yokomatsu, S. Shibuya, and S. Soeda. 2007. Inhibition of lipopolysaccharide-induced release of interleukin-8 from intestinal epithelial cells by SMA, a novel inhibitor of sphingomyelinase and its therapeutic effect on dextran sulphate sodium-induced colitis in mice. *Cell. Immunol.* 245:24–31.

Sano, Y., F.E. Gomez, J.L. Hermsen, W. Kang, J. Lan, Y. Maeshima, and K.A. Kudsk. 2008. Parenteral nutrition induces organ specific alterations in polymeric immunoglobulin receptor levels. *J. Surg. Res.* 149:236–242.

Schromm, A.B., K. Brandenburg, H. Loppnow, U. Zahringer, E.T. Rietschel, S.F. Carroll, M.H. Koch, S. Kusumoto, and U. Seydel. 1998. The charge of endotoxin molecules influences their conformation and IL-6-inducing capacity. *J. Immunol.* 161:5464–5471.

Simpson, N., R. Shaw, V.F. Crepin, R. Mundy, A.J. FitzGerald, N. Cummings, A. Straatman-Iwanowska, I. Connerton, S. Knutton, and G. Frankel. 2006. The enteropathogenic *Escherichia coli* type III secretion system effector Map binds EBP50/NHERF1: implication for cell signalling and diarrhoea. *Mol. Microbiol.* 60:349–363.

Sjoqvist, U., E. Hertervig, A. Nilsson, R.D. Duan, A. Ost, B. Tribukait, and R. Lofberg. 2002. Chronic colitis is associated with a reduction of mucosal alkaline sphingomyelinase activity. *Inflamm. Bowel Dis.* 8:258–263.

Slight, I., M. Bendayan, C. Malo, E. Delvin, M. Lambert, and E. Levy. 2004. Identification of microsomal triglyceride transfer protein in intestinal brush-border membrane. *Exp. Cell Res.* 300:11–22.

Soo, I., K.L. Madsen, Q. Tejpar, B.C. Sydora, R. Sherbaniuk, B. Cinque, L. Di Marzio, M.G. Cifone, C. Desimone, and R.N. Fedorak. 2008. VSL#3 probiotic upregulates intestinal mucosal alkaline sphingomyelinase and reduces inflammation. *Can. J. Gastroenterol.* 22:237–242.

Staneva, G., M.I. Angelova, and K. Koumanov. 2004. Phospholipase A2 promotes raft budding and fission from giant liposomes. *Chem. Phys. Lipids.* 129:53–62.

Su, F., R. Brands, Z. Wang, C. Verdant, A. Bruhn, Y. Cai, W. Raaben, M. Wulferink, and J.L. Vincent. 2006. Beneficial effects of alkaline phosphatase in septic shock. *Crit. Care Med.* 34:2182–2187.

Tabb, D.L., C.G. Fernando, and M.C. Chambers. 2007. MyriMatch: highly accurate tandem mass spectral peptide identification by multivariate hypergeometric analysis. *J. Proteome Res.* 6:654–661.

Tan, S., and S.C. Hooi. 2000. Syncollin is differentially expressed in rat proximal small intestine and regulated by feeding behavior. *Am. J. Physiol. Gastrointest. Liver Physiol.* 278:G308–G320.

Teichgraber, V., M. Ulrich, N. Endlich, J. Riethmuller, B. Wilker, C.C. De Oliveira-Munding, A.M. van Heeckeren, M.L. Barr, G. von Kurthy, K.W. Schmid, et al. 2008. Ceramide accumulation mediates inflammation, cell death and infection susceptibility in cystic fibrosis. *Nat. Med.* 14:382–391.

Tokuo, H., and M. Ikebe. 2004. Myosin X transports Mena/VASP to the tip of filopodia. *Biochem. Biophys. Res. Commun.* 319:214–220.

Tyska, M.J., and M.S. Mooseker. 2004. A role for myosin-1A in the localization of a brush border disaccharidase. *J. Cell Biol.* 165:395–405.

Tyska, M.J., A.T. Mackey, J.D. Huang, N.G. Copeland, N.A. Jenkins, and M.S. Mooseker. 2005. Myosin-1a is critical for normal brush border structure and composition. *Mol. Biol. Cell.* 16:2443–2457.

van Veen, S.Q., A.K. van Vliet, M. Wulferink, R. Brands, M.A. Boermeester, and T.M. van Gulik. 2005. Bovine intestinal alkaline phosphatase attenuates

the inflammatory response in secondary peritonitis in mice. *Infect. Immun.* 73:4309–4314.

Xie, Q., and D.H. Alpers. 2000. The two isozymes of rat intestinal alkaline phosphatase are products of two distinct genes. *Physiol. Genomics.* 3:1–8.

Zhang, B., S. Kirov, and J. Snoddy. 2005. WebGestalt: an integrated system for exploring gene sets in various biological contexts. *Nucleic Acids Res.* 33:W741–W748.

Zhang, H., J.S. Berg, Z. Li, Y. Wang, P. Lang, A.D. Sousa, A. Bhaskar, R.E. Cheney, and S. Stromblad. 2004. Myosin-X provides a motor-based link between integrins and the cytoskeleton. *Nat. Cell Biol.* 6:523–531.